Vortex Lattice Method Investigation of Tip-Leakage Flow

Christophe Montsarrat, Jérôme Boudet

VORTEX LATTICE METHOD INVESTIGATION OF TIP-LEAKAGE FLOW

Christophe Montsarrat
Safran Aircraft Engines
Moissy-Cramayel, France
and
Ecole Centrale de Lyon, CNRS,
Universite Claude Bernard Lyon 1, INSA Lyon
LMFA, UMR5509
69130, Ecully, France
Mail: christophe.montsarrat@edf.fr *

Jérôme Boudet
Ecole Centrale de Lyon, CNRS,
Universite Claude Bernard Lyon 1, INSA Lyon
LMFA, UMR5509
69130, Ecully, France
Mail: jerome.boudet@ec-lyon.fr

* *The author now works in the fluid mechanics department of EDF R&D, 78400 Chatou, France.*

Abstract

The use of a Vortex Lattice Method (VLM) is investigated on a tip-leakage flow single blade configuration (NACA 0012) for a wide range of tip gaps. The aim is to estimate the circulation of the tip-leakage vortex (TLV) detaching from the blade. The evaluation of that circulation without adding viscous effects to the potential method is comparable with the experimental measurements for the largest gaps but requires a diffusive model for the smaller gaps. A new diffusive model is constructed and integrated to the VLM, yielding a very good match with the experiment on the circulation for the whole tip gap range. This result indicates that for thin blades, the development of the TLV can be described in two stages: (i) a potential formation, (ii) a viscous diffusion leading to a decay once the vortex is detached from the blade.

1 Introduction

1.1 Tip-leakage flow

Although it is a well-known phenomenon in turbomachinery, the understanding and modelling of tip-leakage flow (TLF) remains a challenge in the domain. A significant performance increase could be achieved by reducing the intensity of the phenomenon, strictly speaking. Two concrete illustrations of negative effects of TLF can be brought up:

1. It has a significant impact on the compressor, even contributing up to 30% of the losses [1]. It affects both the mass flow rate and the compression ratio that can be significantly reduced by an intense TLF.
2. It can play a crucial role in the onset of instabilities, such as rotating stall [2] [3], thus reducing the operating range of the compressor.

TLF is encountered at the tip of rotor blades of compressors or turbines. The pressure difference across the rotor blades generates a leakage flow in-between the blade tip and the casing wall, that mixes up with the mainstream flow, where the leakage flow rolls up into the tip-leakage vortex (TLV), as shown in Figure 1. The present paper rather focuses on compressor-alike configurations, for which the blade thickness is much lower than the chord length.

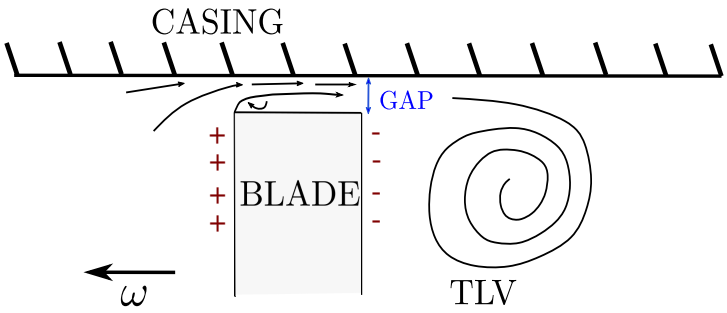

Figure 1: Schematic on the formation of the tip-leakage vortex.

Most of the design choices have to be made during the preliminary phases of design, when a wide variety of designs are explored. During this phase, the TLF modelling needs to be ro-

bust and accurate, with a limited computational cost. Reviewing the literature, one can roughly divide the existing types of TLF modelling into three categories:

1. The leakage flow within the gap ends up mixing up with the mainstream flow, which generates losses [1] [4]. By estimating the angle between the leakage flow and the mainstream flow, and the section area ratio between the two streams, Storer and Cumpsty [4] were able to compute total pressure losses due to TLF.
2. TLF affects the development of the boundary layer at casing. Smith [5] showed how it influences the growth of the boundary layer and hence the loading of the blade in the tip region. Koch and Smith [6] had previously shown how integral values of the casing boundary layer could be estimated iteratively, in order to calculate the resulting losses. There are a few models considering the *blockage*, defined by the restriction of the effective section area, caused by the boundary layers. Khalid's model [7] showed how the increase of the blockage coefficient directly affects the total pressure deficit and the losses. He clearly evidenced the relation between a more intense TLF and losses, also causing more blockage.
3. The third type of models consists in observing the development of the tip-leakage vortex formed once the TLF has rolled up and detached from the suction side. The vorticity field associated to the presence of the TLV is responsible for losses through the deviation of the streamlines. Because of the deviation, the deflection normally achieved by the blade without the TLV is reduced, which induces a reduction of the blade loading. Several models are therefore interested in estimating the circulation of the TLV, corresponding to the integral value of the vorticity field. Lakshminarayana and Horlock's model [8] makes use of the lifting line theory in order to calculate the circulation of the vortex formed in the gap of a slotted wing. Nikolos *et al.* [9] estimated the leakage flow in the gap for a cascade in order to calculate the circulation of the generated TLV. Modelling its diffusion with analytical vortices enabled the calculation of the total pressure loss related to the vorticity distribution.

1.2 Formation of the tip-leakage vortex

Rains [10] was one of the first to model the tip-leakage flow. One of the main assumptions he made was on the pressure gradients, assumed to be much greater pitchwise than streamwise. Following this assumption, the tip-leakage flow can essentially be divided into two main regions: (i) The *vena contracta* inside the gap, due to a flow separation on the blade tip. (ii) The region where the rolling up of the leakage flow occurs, followed by the diffusion and the decay of the TLV downstream. The work of Chen [11] provides a criterion to state whether the leakage flow within the clearance can be considered inviscid. Based on the thickening of the boundary layer developing in the clearance and the tip gap size, his conclusions indicate that the process can be considered as inviscid in the clearance.

Figure 2 illustrates how characteristics of the TLV, in a blade-to-blade view, affect the compressor performance. The point of detachment (indicated by D) combined to the trajectory of the detaching TLV is a first indicator of the performance loss induced by the presence of the TLV: the closer D is to the leading edge, the more losses [12–15]. Indeed, as shown in the figure, the vorticity from the TLV invades more and more the passage, generating more losses. Also, from Vo *et al.* [3], Yamada *et al.* [16], Tan *et al.* [17], the impingement of the TLV on the neighbouring blade can trigger instabilities. Finally, the size and intensity of the TLV are quantified by its circulation. This latter characteristic is discussed in the following section as it is the main focus of the present work. Overall, it can be seen that the performance is drastically lowered when the TLV gets closer to the leading edge of the neighbouring blade ($\varepsilon_2 > \varepsilon_1$) or when the circulation Γ increases. From the literature, the position and trajectory of the TLV relate to the stability of the compressor, while the circulation is a direct indicator of the losses on performance.

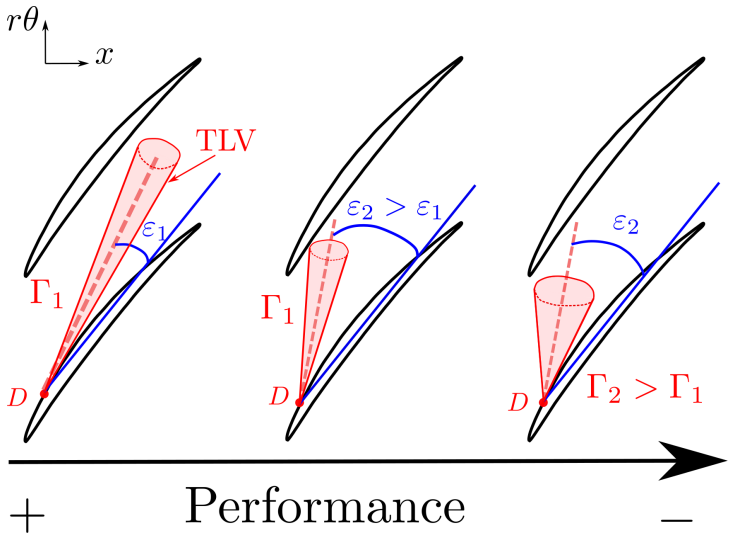

Figure 2: Effect of the position and the intensity of the TLV in a rotor passage on the compressor performance. The TLV circulation is noted Γ (with values $\Gamma_1 < \Gamma_2$), the detachment point is noted D, and the TLV angle is noted ε (with values $\varepsilon_1 < \varepsilon_2$).

1.3 Main influences on the tip-leakage vortex

In order for a designer to optimize the shape of a blade regarding TLF, it is necessary to understand how TLF is affected by variations of geometric and flow parameters. In the literature, most studies focus on the blade loading, the effect of the

boundary layer at casing, and the tip gap size. When the blade is more loaded, the tip-leakage flow has a tendency to be more intense and with a trajectory that is closer to the neighbouring blade. Courtiade [2], in his experimental study of a high-pressure compressor, clearly observed this tendency between two operating points with numerous unsteady measurements. The numerical study of Riéra [13] with a zonal detached-eddy simulation (ZDES) confirmed these results on the same compressor. His observations concerned the circumferential extension of the TLV, larger for the more loaded operating point. He also showed that the TLV was shifted upstream, closer to the neighbouring leading edge. The work of Vo *et al.* [3] showed that the spillage of the TLV upstream of the neighbouring leading edge could trigger the first cell of a rotating stall, if also combined to a backflow at the trailing edge.

Concerning the effect of the casing boundary layer, the conclusions of Brandtl *et al.* [12], on the increase of the thickness of the boundary layer, concerned the point of detachment of the TLV, that gets closer to the leading edge. Deveaux *et al.* [18] showed that the effect was also clear on the trajectory of the TLV, that moves away from the suction side. These two results illustrate the detrimental effect of an increase of the boundary layer thickness for the performance, according to Figure 2.

Regarding the tip gap size, Cumpsty [19] showed how detrimental the rise in size could be for a compressor in terms of operating range and efficiency. This can be related to the evolution of the TLV characteristics. The experiments of Doukelis *et al.* [20], on an annular cascade, indicated a growth in the TLV size along with an increase of the losses in the tip region. They however also showed that the TLV detaches closer to the trailing edge for an increased gap. Kang and Hirsch [21] made the same observations on their experiment with NACA65 airfoils. On an axial compressor rotor, Inoue *et al.* [22] drew the same conclusions. The experiment of Deveaux *et al.* [18] on a NACA0012 airfoil and its numerous measurements showed the significant impact of the tip gap size on the circulation of the TLV, which increases. It also confirmed the fact that the TLV trajectory is farther away from the suction side, but detaches further downstream with the increase of the tip gap size.

1.4 Motivation

Our final objective is to develop a low-order tool, quick and accurate enough for preliminary design, able to predict accurately the three characteristics of the TLV with the main sensitivities. In particular, the present article focuses on the developments of our module, called *PyLiSuite*, using the vortex lattice method (VLM) to predict the sensitivity of the TLV intensity (its circulation) to the tip gap size τ.

Appendix A illustrates the relation between the circulation and the compressor performance, which can be summarized in two main points:

1. Relation (17) directly shows that in nominal conditions, where the flow can reasonably be assumed to be axisymmetrical, the circulation around the blade at a given radius is a direct indicator of the work done by the blade.
2. In the tip region, the influence of the TLV, due to its vorticity field, disturbs the velocity field and impacts the work that would be produced by the blade without the TLV. Correctly predicting the circulation of this vortex and the velocity field enables to estimate the work deficit due to the presence of the TLV.

The motivation for choosing the VLM stems from these two observations and the necessity to maintain a low computational cost. The present paper is intended to show that an accurate evaluation of the TLV circulation can be obtained with such a method. The VLM method is described and the main developments to extend it to TLF are explained. In particular, a new viscous diffusive model is presented and combined with the VLM.

2 Development of the Vortex Lattice Method (VLM)

Potential methods are primarily based on the assumption that the flow considered is inviscid, irrotational and incompressible. Following these assumptions, the flow equations simply reduce to a Laplace equation on the potential Φ of the velocity $\boldsymbol{V}$:

$$\Delta\Phi = 0 \quad \text{where:} \quad \boldsymbol{V} = \boldsymbol{\nabla}\Phi \tag{1}$$

Thanks to the linearity of Laplace equation, it can be solved by combining elementary solutions distributed over the body considered and solving a linear system. This kind of methods has been commonly used in external aerodynamics [23], for the preliminary design of aircrafts for example, and has the advantage of being quick and accurate.

For internal flows however, the use of potential methods is far less common. Regarding specifically TLF, only few have tried to use them in the literature. Lakshminarayana and Horlock's model [24] is one of the first article to deal with TLF by using the lifting line theory of Prandtl [25], which derives from the potential theory through further assumptions on the dimensions of the aerodynamic body. Applied to a slotted wing with an adjustable midspan gap, a model of TLF, the method yielded satisfying results for large tip gaps such as $\tau/c > 1$, but showed limitations for smaller gaps. By introducing a retained vorticity coefficient K, they were able to improve the results for gaps lower than one chord length. This coefficient accounts for the viscous effects not reproduced by the lifting line theory, but was determined empirically. Another limitation of the method lies in the application to compressor blades themselves, that usually present a low aspect ratio, with a span length of the same order

of magnitude as the chord length. Indeed, the fact that the span is much greater than the chord is an important prerequisite for the lifting line theory. The present work aims at showing what a more generic potential method like the Vortex Lattice Method (VLM), introduced in the following section, can bring when applied to TLF.

2.1 General presentation of the VLM

If the lifting line theory consists in reducing the aerodynamic body to a distribution of vortices along a span line, the VLM discretization is two-dimensional. Vortices of undetermined circulations are distributed along the chordwise and spanwise directions. The application of the non-penetration condition $\boldsymbol{V} \cdot \boldsymbol{n} = 0$ to the control points discretizing the surface leads to the resolution of a linear system to calculate the unknown circulations. Figure 3 shows the discretization of a flat plate with horseshoe vortices (HSV), the type of singularity used for the present VLM. Each HSV consists of three branches, one bound to the surface (the *head*) and two extending downstream to infinity (the *legs*). Considering the HSV represented in the figure: the bound branch has a circulation Γ_{AB} while the two legs have respective circulations $\pm\Gamma_{AB}$.

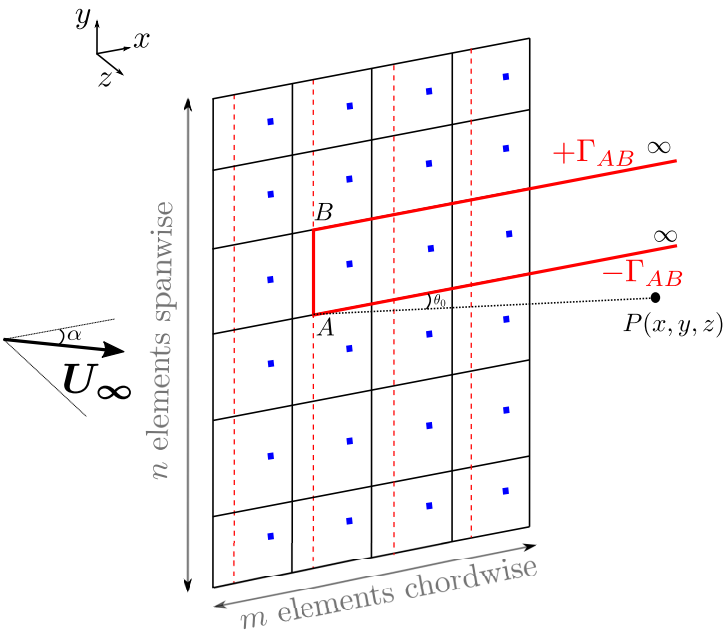

Figure 3: Illustration of the VLM discretization of a flat plate. U_∞ is the freestream velocity and α is the angle of attack.

Different results can be obtained from the knowledge of the distribution of circulation over the surface. First, following Helmholtz's theory, the shed circulation can be computed and related to the spanwise variation of circulation. This is of interest for the present work, focusing on the circulation of the shed TLV. Second, the induced velocity due to the circulations can be calculated anywhere in the flow field with Biot-Savart's law [23]. This may be used to predict the leakage flow through the gap.

In the context of compressor blades, the importance of using VLM instead of the lifting line theory must be stressed: (i) VLM does not require an assumption on the aspect ratio of the blade, (ii) Introducing a tip gap in the lifting line theory, there is a contradiction with the line discretization since the tip gap introduces a smaller length scale than the chord length itself.

The validation of the method, implemented in the module called *PyLiSuite*, was thoroughly explained in a previous paper by Montsarrat *et al.* [26], in the context of external aerodynamics. Here, the focus is on the application to tip-leakage flows and the developments made in the context of turbomachinery.

2.2 Application to tip-leakage flow

The cylindrical configuration is approximated as a linear cascade, with blades enclosed between a flat hub and a flat casing. Similarly to Lakshminarayana and Horlock's model, the case of a blade tip distant by τ from the casing wall is reproduced with VLM by considering two mirror blades 2τ away from one another. The hub is also accounted for by applying a mirror condition to the original blade with no gap. Figure 4 shows such a configuration for a flat plate with a span length b. Two main ideas explain this choice:

1. There is no shed vorticity at the hub that would be due to the formation of a potential vortex. With the potential theory, this means that the spanwise slope of the circulation is zero at the hub ($d\Gamma/dy = 0$).
2. The non-penetration condition is applied to the casing wall by mirroring the same set (blade + hub mirror blade), ensuring that the normal velocity component is zero at casing, by symmetry.

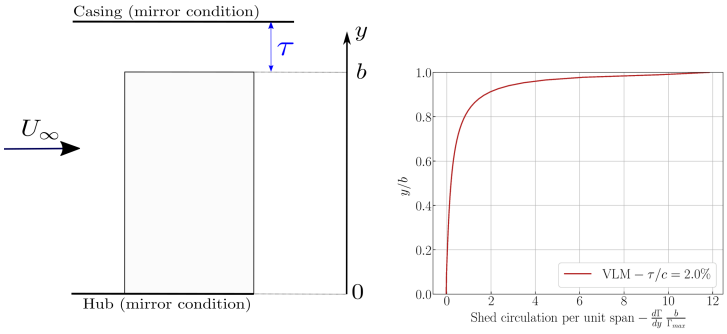

Figure 4: Application of VLM to tip-leakage flow.

The resulting distribution of shed circulation is illustrated in Figure 4.

Following the preliminary study in [26], progress has been made on the application of the VLM to TLF. First, a criterion on the grid size with respect to the tip gap τ has been developed. Indeed, the results on the circulation are very sensitive to the grid. The chordwise grid distribution is based on a bigeometric distribution with an expansion ratio $g = 1.05$ and a minimum cell size $\Delta_{0,c}$. The number of points is set to 37 after varying the ratio $c/\Delta_{0,c}$. Spanwise, the grid is also based on a bigeometric distribution of expansion ratio $g = 1.05$ and minimum cell size at the tip $\Delta_{0,b}$, which is here varied.

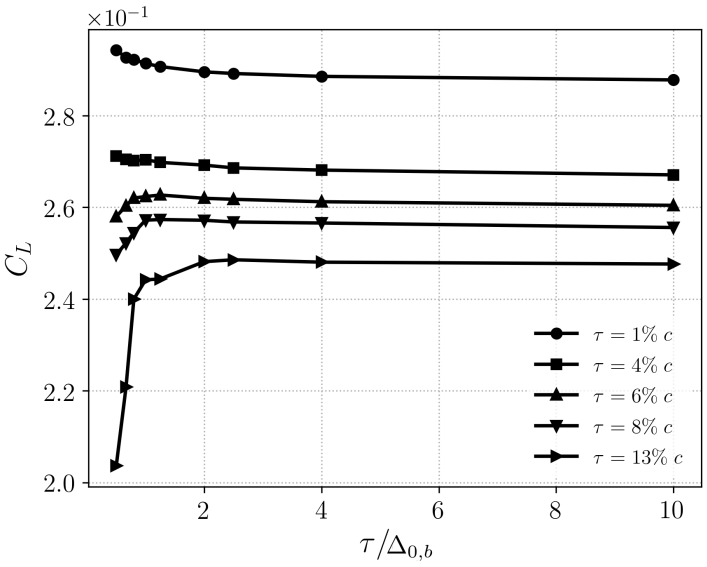

Figure 5: Evolution of the lift coefficient on a flat plate, with an aspect ratio $AR = 1$ and $\alpha = 5°$, for different values of τ.

The grid convergence is assessed through the evolution of the lift coefficient, computed from the total bound circulation on the blade, with $\tau/\Delta_{0,b}$. From Figure 5, a criterion can be inferred, valid for all the tip gap sizes tested:

$$\tau/\Delta_{0,b} > 2. \tag{2}$$

The criterion obtained is physically sound: the smaller the tip gap, the finer the discretization must be.

2.3 Computational performance of *PyLiSuite*

The VLM here presented has been developed with only one type of singularities. Horseshoe vortices are chosen to capture the shed vorticity of the TLV. They are distributed over the camber surface of the blade and the circulations are computed by solving the linear system presented before. The thickness is not considered in the current method since its effect is considered to be second order. Indeed, the thickness of compressor blades is generally small and the loading distribution is mostly due to the camber (local deflection).

The architecture of the code is in *Python* but the linear system is constructed in *Fortran*. This enables a much more efficient computation compared to a code fully written in *Python*. The computational time for a standard grid size on a single CPU core is about 30 seconds. The capability of the method to run much quicker (a few seconds) than a RANS simulation (a few dozens of minutes) constitutes one of the main motivations of the present work, particularly for preliminary design.

3 Modelling of the TLV diffusion

Up until this section, the method developed has not considered any viscous effect. When it comes to external aerodynamics and the prediction of lift on aircraft wings and fuselage or the induced drag generated by them, VLM has proved over the years its efficiency to combine good accuracy and low cost. It is still nowadays used by aircraft designers in the early steps of design. However, getting into wall-bounded flows, the use of that kind of potential method is seldom in the literature: for a sufficient accuracy with this type of flows, viscous effects cannot be neglected and the pure potential method is then insufficient. The example of Lakshminarayana and Horlock's model [24] is notable, with the introduction of a retained vorticity coefficient. In fact, this coefficient accounts for viscous effects for the smallest tip gaps. In the case of turbomachinery flows, these effects must be considered because boundary layers and secondary flows represent a significant part of the losses.

Rains' [10] and Chen's [11] assumptions are crucial for the rest of this section. The formation of the TLV is purely potential within the tip gap and the viscous diffusion of the TLV begins as soon as the TLV detaches from the suction side of the blade. This is the main idea behind the viscous model introduced in this paper to predict the intensity of the TLV depending on the tip gap size: the VLM evaluates the total circulation of the TLV *when it detaches from the blade* and its diffusion and decay are predicted by an added viscous correction.

3.1 Viscous diffusion of a vortex dipole

In the VLM, the wake and the TLV consist of the legs of the HSV, distributed along the span. These legs are concentrated vorticity with a constant circulation. The purpose of the additional model is to represent the spatial diffusion of these vorticities. The model is built by considering the interaction of two vortices of opposite circulation, representing one elementary vortex from

the TLV and its mirror vortex in the casing. It is important to notice that in the viscous model, the casing wall is still represented by a slip condition, through the use of a mirror vortex. Physically, this means that the viscous effects are only introduced in the TLV, not on the casing (no boundary layer development).

Van Geffen and Van Heijst performed numerical simulations on the viscous diffusion of a two-dimensional Lamb vortex dipole [27]. Their analysis was done following experiments on vortex dipoles whose characteristics are well described by Lamb's vortices [28]. Their study shows that the two-dimensional Lamb dipole moves along a straight line with a decreasing velocity $U(t)$ and an increasing radius $R_c(t)$, compared to an inviscid vortex pair that also moves along a straight line but with a constant drift velocity U_{drift} and a constant radius. The dipole evolution over time can be divided into two main phases:

1. The radii of the two initially concentrated vortices (of radius R_{c0} and separation τ) grow at the same pace until they reach $R_c(t) = \tau$. This core radius growth is well described by the viscous diffusion model:

$$R_c^2(t) = R_{c0}^2 + 4\nu t \tag{3}$$

2. The two vortices collide and the circulations of both vortices decrease over time, resulting in trails of vorticity shed behind the dipole.

The authors also showed that starting from different types of vortex pairs, not necessarily Lamb alike, the structure of the vortex pair naturally evolves towards a Lamb dipole.

The Direct Numerical Simulation (DNS) of Delbende and Rossi [29] confirms these results: the circulation magnitude of each vortex is also found to decrease over time due to the vorticity trails formed.

3.2 Estimation of the eddy viscosity

The action of the molecular viscosity ν to explain the diffusion of turbulent vortical structures is insufficient. An illustration is the trailing vortices downstream of an airplane wing that are being diffused. Only considering a molecular viscosity to represent their diffusion until their decay results in a much longer time than physically observed. Hence, the effect of turbulence must be taken into account. Squire [30] therefore proposed to replace the molecular viscosity ν by an apparent eddy viscosity $\nu_t \gg \nu$ to model the diffusion and decay of a trailing vortex. In his model, the eddy viscosity can be calculated based on the circulation Γ following this equation:

$$\nu_t = \alpha\Gamma, \tag{4}$$

where α is a constant.

Owen [31] extended Squire's model to represent the decay of a turbulent trailing vortex of circulation Γ by calculating α as:

$$\alpha = \Lambda^2 \left(\frac{\Gamma}{\nu}\right)^{-1/2}, \tag{5}$$

with Λ a constant. His idea was to add a dependency on the Reynolds number, based on the circulation, $Re_\Gamma = \Gamma/\nu$. This model allowed a better agreement with the wind tunnel and flight observations of wing-tip vortices.

The characteristics of Owen's turbulent vortex are very similar to those of Lamb's vortex. In particular, the evolution of the circumferential velocity as a function of the radius is nearly the same. The growth of the core radius R_c with time can be modelled by:

$$R_c = \sqrt{4\nu_t\, t}. \tag{6}$$

The axial vorticity for a vortex of circulation Γ can be written as a function of the distance to the core r:

$$\omega_x(r,t) = \frac{\Gamma}{2\pi R_c^2} e^{-r^2/R_c^2}, \tag{7}$$

with a core radius varying as in (6), and the eddy viscosity ν_t calculated with equations (4) and (5).

3.3 Construction of the new viscous model for an elementary vortex

3.3.1 Interaction of two diffusing mirror vortices

The present model is inspired by grid-free methods to represent incompressible boundary layers, such as Chorin's [32] and Porthouse and Lewis [33]. In such models, a system of point vortices is generated step by step and is subjected to small random displacements. By resorting to a mirror image technique across the wall, the vortices of opposite circulations may annihilate each other in their random displacements. The results obtained by the authors are in good agreement with the Blasius boundary layer growth. Regarding turbulent boundary layers, Chorin advocates to replace the molecular viscosity by an eddy viscosity. Lewis [34] used the same method with Rankine vortices whose radii grow over time through viscous diffusion.

In the present model, two physical effects are represented: (i) the turbulent diffusion of the vorticity, originally concentrated in one line with the VLM, (ii) the interaction with the wall. This is achieved by replacing any line vortex from the VLM by a diffusive pair of vortices, mirrored by the casing. Instead of con-

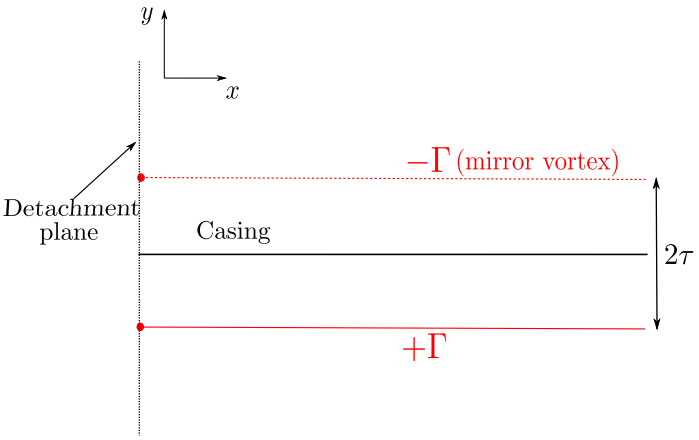

Figure 6: Interaction of two potential mirror vortices.

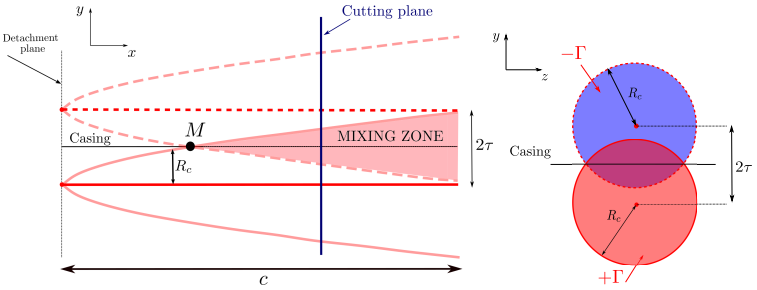

(a) Advection and diffusion of the vortex pair.

(b) Mixing at a given axial position, in the cutting plane.

Figure 7: Sketch of the advection, diffusion and mixing of two mirror vortices of circulation Γ.

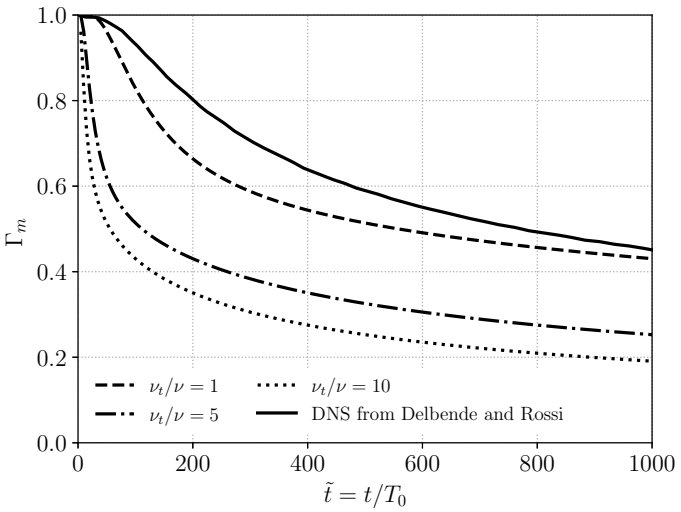

Figure 8: Evolution of the normalized vortex circulation Γ_m as a function of $\tilde{t} = t/T_0$, with $T_0 = 4\tau^2/\Gamma$. The DNS evolution is extracted from [29].

centrating all the vorticity in a single point (the core) at a given abscissa, as represented in Figure 6, it is distributed over a disc of radius R_c. The diffusion is envisaged through Lamb's vortex formulation, using an apparent eddy viscosity.

At a given position x, the advection time from the detachment point x_D is used:

$$t(x) = \frac{x - x_D}{U_\infty}. \tag{8}$$

Figure 7a shows how the radius growth is taken into account in predicting the superposition of the two vortices in the tip region. The circulations $\pm\Gamma$ diffuse at the same pace from the detachment point and eventually collide at point M in the figure. Farther downstream, they have started mixing out, which is shown in the cutting plane (y, z) in Figure 7b. In the proposed model, the circulation of the lower (physical) vortex can be calculated at each axial position, by substracting the influence of the mirror vortex, and integrating the vorticity up to the casing.

From position M, because both vortices keep advecting and diffusing at the same pace, the lower vortex circulation is going to decrease because the opposite vorticity affects more and more the tip region. This models the decrease of circulation described in section 3.1. When the gap size τ increases, the point M moves farther downstream and the circulation of the vortex starts decreasing farther downstream.

3.3.2 Comparison of the circulation decrease to the DNS In this section, the simple model introduced above is compared to the physical decrease captured by the DNS of Delbende and Rossi [29], introduced before. Figure 8 shows the decrease of the normalized circulation Γ_m of each mirror vortex, resulting from their mixing. This is plotted over the dimensionless time for different values of ν_t/ν in the model. The DNS case is laminar, with $Re_\Gamma = \Gamma/\nu = 2500$. Thus, the model with $\nu_t/\nu = 1$ is to be considered for comparison with the DNS. The tendency of the decrease is the same but the model underestimates the resulting circulation of the vortex compared to the DNS, overestimating the circulation decrease over time. When the viscosity ratio is artificially increased to $\nu_t/\nu = 5$ or 10, in order to evaluate the sensitivity of this parameter, the circulation decreases, as expected.

Overall, the simple model with the properly calibrated $\nu_t/\nu = 1$ allows a fairly good prediction of the circulation decrease of a vortex dipole, with only a moderate underestimate of the circulation.

3.4 Integration with VLM

Consider an elementary vortex of initial circulation Γ, detached from a given axial position along the chord. Its circulation at the trailing edge Γ_{TE} depends on τ:

- If the gap is null, the circulations cancel each other out and $\Gamma_{TE} = 0$. As expected, there is no TLV in this case.
- For a small gap, the two vortices start mixing out upstream of the trailing edge and the resulting $\Gamma_{TE} < \Gamma$. The circulation at the trailing edge is larger with a larger tip gap.
- For a very large gap, the two vortices do not cross the casing wall and never collide: $\Gamma_{TE} = \Gamma$ at the trailing edge.

As previously explained, the main benefit of utilizing the VLM, compared to the lifting line theory, is the chordwise discretization. Hence, the chordwise distribution of circulation is a result from VLM for every spanwise position. In particular, it is possible to calculate the chordwise distribution of shed circulation at the tip. The total circulation shed at the tip Γ_{tot}^{shed} is the sum of each shed circulation at position x_i:

$$\Gamma_{tot}^{shed} = \sum_{i=1}^{m} \Gamma_i^{shed}. \tag{9}$$

The shed circulation Γ_i^{shed} results from the integration of $d\Gamma/dy$ over the whole span. Indeed, as shown by Figure 4, the shed circulation is essentially due to the variation of Γ in the vicinity of the tip. The contribution of the inviscid wake is neglected, for every axial position.

The diffusive model can be applied to the shed circulation distribution at the tip, obtained from the VLM:

1. The eddy viscosity $\nu_{t,i}$ for the i^{th} vortex pair, as soon as it detaches from the blade, at x_i, is specified or computed from (4) and (5).
2. The axial vorticity $\pm\omega_{x,i}$ of each vortex of the dipole is calculated based on Lamb's diffusive model.
3. The integration of the axial vorticity in the tip region, downstream of the position x_i, is done as described by Figure 7. This yields $\Gamma_i(x)$.
4. The resulting axial evolution of $\Gamma_{TLV}(x)$ consists of the sum of all the circulations at the position x:

$$\Gamma_{TLV}(x) = \sum_{i=1}^{i(x)} \Gamma_i(x), \tag{10}$$

where $i(x)$ is such that $x_{i(x)} < x < x_{i(x)+1}$.

It must be noted that the development of each dipole is independent from the others, which means that the interactions are not accounted for here.

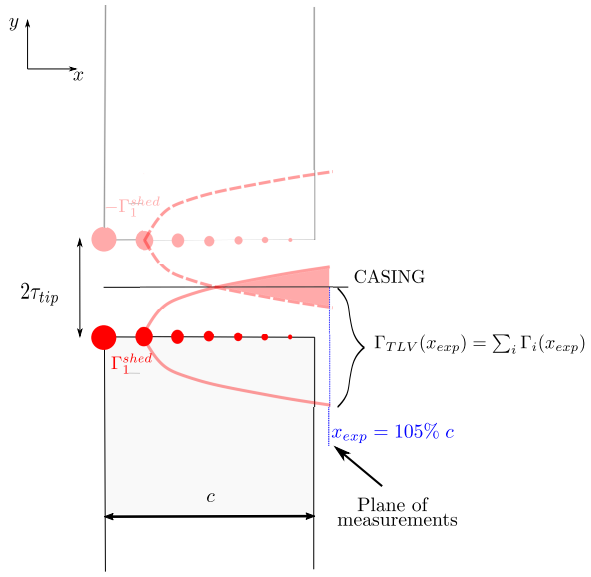

Figure 9: Illustration of the diffusion model applied to the chordwise distribution of shed circulation predicted by VLM.

Figure 9 shows an illustration of the diffusive model applied to VLM. The idea is to use the mixing model on each pair of mirror vortices as it is advected downstream. The diffusion of each elementary dipole is phase-lagged with the next one and even more with the next one, and so on. The resulting circulation of the TLV is therefore a function of x/c and consists of the contribution of each vortex dipole coming from upstream. The chordwise discretization enables to integrate physical characteristics of the TLV, fed by smaller vortices, first gaining a lot of energy near the leading edge [7] and slowly increasing in intensity down to the trailing edge, before decaying further downstream.

4 Application to a TLF configuration

In this section, the VLM combined with the diffusive model, referred to as VLMwdm in the rest of the paper, is tested and compared with experimental and numerical results obtained by Deveaux *et al.* [18] [35]. The evolution of the TLV circulation with the tip gap size τ is investigated for a single blade in a tip-leakage flow configuration. The experimental test rig is introduced below.

4.1 Presentation of the experimental rig *S2I*

The rig consists of a single blade (NACA0012 airfoil) whose distance between the tip and the endwall can be adjusted. The tip gap size varies between 0.5% and 13% chord length. This range of tip gap sizes goes from sizes representative of actual compressors (up to $\approx 4\%\,c$) to larger tip gaps where viscous effects have

much less impact. Figure 10 shows the experimental setup with the variable tip gap size τ. Table 1 summarizes the main parameters of the experiment. More details on the test rig can be found in [18]. The angle $\alpha = 10°$ was chosen so that the blade was sufficiently loaded without getting too close to stall. The objective was to be able to observe an intense TLV.

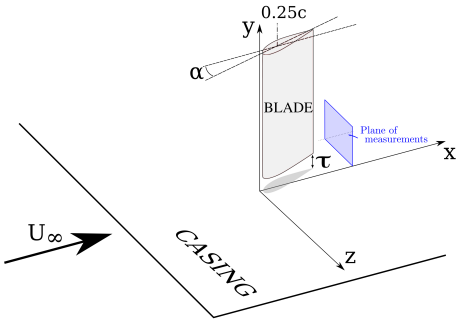

Figure 10: Sketch of the tip-leakage flow configuration *S2l*.

U_∞	40 m/s
Re	550 000
M_∞	0.1
P_∞	101325 Pa
Tu	0.07%
Chord length c	200 mm
Span b	560 mm
Angle α	10°
τ/c	From 0.5% to 13%

TABLE 1: Main parameters of the *S2l* experiment.

Experimental measurements As indicated in Figure 10, the measurements are taken right downstream the trailing edge in the plane $x = 1.05c$. Five-hole probes are used to measure the flow velocity components and calculate the axial vorticity. The incoming boundary layer at casing selected for the present study is characterized by a momentum thickness $\theta/c = 0.6\%\,c$. The corresponding boundary layer thickness is $\delta = 4.95\%\,c$, which given the tip gaps considered (see Table 2), immerses the whole gap region for six of the nine cases.

The circulation of the TLV is calculated by integrating the axial vorticity. It is indeed asssumed that most of the TLV vorticity is in the axial direction. Besides, only the positive axial vorticity is considered to make sure the induced vortex is not included in the TLV circulation. More details can be found in [18].

τ/c (%)	0.5	1	1.5	2.5	3.5	4.5	6	8	13

TABLE 2: Tip gap sizes tested with VLM on *S2l*.

Results from RANS simulations using the RSM SSG/LRR-ω turbulence model, obtained by Deveaux [18], are also used in this section to analyze the axial evolution of the TLV circulation.

4.2 Prediction of the circulation

The evolution of the circulation of the tip-leakage vortex with the tip gap size is shown in Figure 11. It compares the TLV circulation from the five-hole probes measurements and the RANS simulations, the shed circulation from the VLM, and the TLV circulation from the VLMwdm (for three values of ν_t/ν).

The first thing that can be observed in the measurements is the large increase of the circulation with the tip gap size: the larger is the gap, the more intense is the TLV. However, this rise is less and less important for the larger gaps. Looking more closely, the circulation reaches a peak at $8\%\,c$ and slightly decreases for the largest gap. Essentially, the circulation for very large gaps reaches a plateau and can be well predicted by potential theory alone (VLM).

The circulation obtained from the VLM for the two largest tip gaps ($\tau/c = 8\%\,c$ and $13\%\,c$) matches the experiment. The method is however inaccurate for smaller gaps: the circulation obtained slightly decreases with the gap size and largely overestimates the experimental TLV circulation. For compressor blades, the range of interest for τ lies between $1\%\,c$ and $4\%\,c$. Note that the results from a previous paper [26], where the VLM was applied, captured incorrectly an increase of the TLV circulation with the tip gap size. The requirements established here on the grid size (see Equation (2)) allowed that result to be corrected.

The VLMwdm results are considered next, for three different values of the viscosity ratio: $\nu_t/\nu = 100$, 200 and 300. The order of magnitude of these values is consistent with the results of Chen *et al.* [36] in the tip gap region of a compressor rotor. For $\nu_t/\nu = 200$, the fit with the experiment is very good for the whole range of gaps. The viscous model preserves the right value of circulation for the largest gaps and significantly improves the results for the smaller gaps, of interest for compressor rotors. Both the levels and the increase rate with the tip gap size are well captured with the VLMwdm. The model fails to capture the slight decrease of the circulation between the two largest gaps, but the error is small compared to the experiment. The specific choice of $\nu_t/\nu = 200$ can be seen as a calibration of the model. However, the sensitivity to this parameter is moderate, as shown by Figure 11. In the context of preliminary design, fairly good results are obtained by simply using a reasonable order of magnitude

$\nu_t/\nu = 100$.

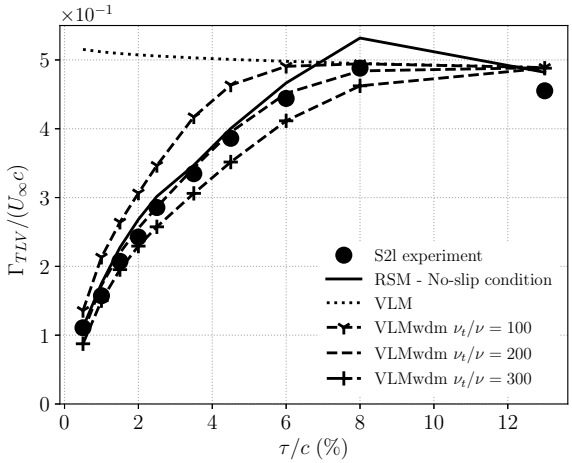

Figure 11: Circulation of the TLV in the plane of measurements ($x = 1.05c$) as a function of τ/c, from the experimental measurements, the RANS RSM simulations, the VLM and the VLMwdm.

4.3 Streamwise evolution of the circulation

The VLMwdm thus enables to capture the circulation as a function of the tip gap size downstream of the blade, where the measurements have been taken. The model can be explored further by investigating the evolution of the circulation along the chord length. The experimental measurements are insufficient for an analysis but the results from the numerical investigation with RANS RSM can be used as a reference.

Considering again Figure 11, the RANS RSM simulations capture very well the experimental evolution, with a slight overestimate for the three largest gaps. This gives confidence for using the results from the RANS RSM simulations as a reference for the axial evolution of the circulation.

Figure 12 shows the axial evolution of the TLV circulation for three different tip gap sizes: $2\%c$, $6\%c$ and $13\%c$, for the RANS simulations and the VLMwdm ($\nu_t/\nu = 200$). The circulation increases along the blade chord ($x/c < 100\%$), by accumulation of shed vorticity. Downstream, in the wake of the blade, the circulation decreases because of viscosity and vortex interaction. This evolution is captured by both the RANS simulations and the VLMwdm. Coherently with the results showed before in the plane of measurements ($x/c = 105\%$), the circulations from the RANS RSM simulations and the VLMwdm intersect at that position.

The slope of the chordwise increase is fairly well captured by the VLMwdm, although the assumption of a vortex detachment starting from the leading edge is clearly wrong. In reality, vorticity can accumulate in the fore part of the gap, within tip-separation vortices, and be shed further downstream. The peak of circulation of the TLV is reached sooner for the smaller gap, at about 75% chord, both with RANS RSM and the VLMwdm. The VLMwdm nonetheless underestimates the maximum circulation at that latter position (0.30 instead of 0.34). For $\tau/c = 6\%$, the amplitude of the peak is also underestimated but the location (at about $90\%c$) is captured by the VLMwdm. For the largest gap, the peak is reached at the trailing edge with both methods, with the same intensity of the vortex.

Finally, the decay of the circulation downstream of the trailing edge is milder with VLMwdm, compared to RANS RSM, for the three tip gap sizes. It is known that numerical schemes and models can be over-diffusive in RANS. This may explain the faster decay of vorticity. Limitations of the VLMwdm are also discussed in the next section.

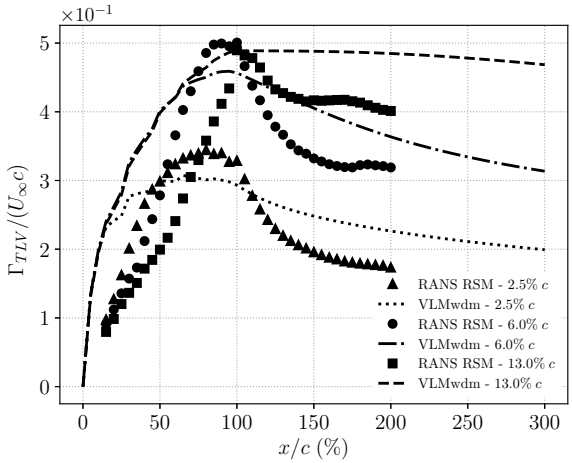

Figure 12: Axial evolution of the circulation Γ_{TLV} for three tip gap sizes, from the RANS RSM simulations and the VLMwdm.

5 Discussions

5.1 Endwall/TLV interaction

The circulation increase with the gap size is modelled by a system of mirror vortices that collide and partially annihilate each other, resulting in a reduction of the total circulation for small gaps. The endwall is only modelled by a slip condition and the consistency of the model is here discussed. To this end, the differences between the interaction of a vortex with an endwall and the interaction of two vortices must be discussed.

First, when the TLV interacts with the casing boundary layer, the spanwise position of the vortex is not fixed. According

to Brion [37], the interaction with a boundary layer pushes the vortex away. This effect is not taken into account in VLMwdm, since the spanwise position of the elementary vortices is fixed. Second, some vorticity of the boundary layer is transported by the vortex. This results in the formation of an induced vortex, of opposite circulation [38], which is not modelled by the VLMwdm.

5.2 Estimation of the eddy viscosity

The use of a system of mirror Lamb vortices enables to reproduce the experimental results with a single calibration on ν_t/ν, quantifying the turbulent diffusion of the initial potential vortices shed along the chord. The value $\nu_t/\nu = 200$ is consistent with the order of magnitude expected for a TLV mixing with a boundary layer in the tip gap region [36].

Representing the TLV as a stable and persistent structure through the diffusion of a Lamb vortex seems to be adapted. Other effects could be modelled by a modification of ν_t/ν, such as the relative motion between the blade and the casing wall, which changes the vorticity distribution and subsequently the total circulation in the tip region. A correlation could also be developed to adapt the value of the viscosity ratio to the thickness of the incoming boundary layer on the casing.

6 Conclusions

In the context of turbomachinery flows, the circulation of the tip-leakage vortex (TLV) is an important source of losses and must be estimated accurately in the first steps of design. The present study has proposed an application of a vortex lattice method (VLM) to estimate the circulation shed from a single blade tip-leakage flow. After introducing the VLM and its adaptation to tip-leakage flows, a new diffusive model has been presented to account for the viscous process influencing the development of the TLV. The motivation was to capture the TLV circulation increase with the tip gap size, as measured experimentally.

The model applied to mirror vortices of circulation $\pm\Gamma$ consists in summing algebrically the contributions of diffused vorticity in the tip region. The circulation shed is not concentrated onto a line as in standard VLM but instead diffuses spatially, following an analytical diffusive vortex distribution. Because the vorticities of the mirror vortices across the casing spread over a growing disc area, they eventually collide and their mixing is accounted for. Moreover, turbulence is accounted for by substituting the molecular viscosity by an eddy viscosity, whose order of magnitude is well-known. From the VLM, the axial distribution of shed circulation can be used as an input for the diffusive model. This mimics the actual physics of the formation of the TLV, that gains in intensity along the chord.

The VLM supplemented with the diffusive model, referred to as VLMwdm, yields very good results on a single blade TLF configuration, in comparison to the experimental measurements. A first achievement of the VLM is its capability to accurately predict the shed circulation for large tip gaps. Although the VLM alone is not capable of predicting the evolution of Γ_{TLV} with the tip gap size, the use of VLMwdm enables to capture the experimental increase of Γ_{TLV} with the tip gap size over the whole range of gaps investigated.

The results achieved by the combination of the VLM with the diffusive model bring an important conclusion on the formation and development of the tip-leakage vortex: for thin blades, the formation of the TLV is essentially a potential process while its development downstream of the detachment point rather responds to a viscous process (diffusion and then decay). This result confirms assumptions made in the literature but never investigated with the use of a vortex lattice method, to the authors' knowledge.

These results are very encouraging to further pursue the developments of that method towards a better representation of tip-leakage flows in turbomachinery with a low-order tool. Historically, this type of methods has achieved very good predictions for external aerodynamics but has never been extended to a preliminary design tool for internal flows. The main advantages are its simplicity combined to a good accuracy and a low computational cost. Further work is needed regarding the periodicity (cascade configurations), compressibility effects, generalized inflow conditions and relative motion between the casing and the blades. Also, the prediction of the trajectory and the detachment point of the TLV would provide valuable information on the performance and operability.

Acknowledgements

The authors are grateful to the team of ONERA Meudon and the authors of [18] for providing the experimental data for this paper. Benjamin Deveaux is particularly thanked for his collaboration during his PhD, which was part of the ANR project NumERICCS (Projet-ANR-15-CE06-0009). The authors are also thankful to Safran Aircraft Engines for funding the PhD of C. Montsarrat.

Nomenclature

α	Angle of attack or diffusion parameter
Γ	Vortex circulation
Γ_m	Normalized circulation of one mirror vortex
$\Delta_{0,b}$, $\Delta_{0,c}$	Minimum cell sizes (spanwise, chordwise)
Λ	Diffusion parameter
ν and ν_t	Molecular and eddy viscosities
τ	Tip gap size

Φ	Potential function
ω	Rotation speed
ω_x	Axial vorticity
ε	Angle between the TLV and the blade camber line
b	Span length
c	Chord length
D	Point of detachment
h_0	Stagnation enthalpy
r	Radial coordinate
R_c	Vortex core radius
Tu	Turbulence intensity
U_∞	Freestream velocity
U	Blade velocity
$\mathbf{V}$	Absolute flow velocity
$\mathbf{W}$	Relative flow velocity
RANS	Reynolds-averaged Navier-Stokes
TE	Trailing edge
TLF	Tip-leakage Flow
TLV	Tip-leakage Vortex
VLM	Vortex Lattice Method
VLMwdm	VLM with diffusive model

References

[1] J. Denton, "Loss Mechanisms in Turbomachines," tech. rep., The American Society of Mechanical Engineers, New York, 1993.

[2] N. Courtiade and X. Ottavy, "Experimental Study of Surge Precursors in a High-Speed Multistage Compressor," *Journal of Turbomachinery*, vol. 135, p. 061018 (9 pp.), Sept. 2013.

[3] H. D. Vo, C. S. Tan, and E. M. Greitzer, "Criteria for spike initiated rotating stall," *Journal of turbomachinery*, vol. 130, no. 1, p. 011023, 2008.

[4] J. Storer and N. Cumpsty, "An Approximate analysis and prediction method for tip clearance loss in axial compressors," *The American Society of Mechanical Engineers*, no. 93-GT-140, pp. 1–10, 1993.

[5] L. H. Smith, "Casing boundary layers in multistage axial-flow compressors," *Flow Research on Blading*, pp. 275–304, 1970.

[6] C. C. Koch and L. H. Smith, "Loss Sources and Magnitudes in Axial-Flow Compressors," *Journal of Engineering for Power*, vol. 98, pp. 411–424, July 1976.

[7] S. A. Khalid, A. S. Khalsa, I. A. Waitz, C. S. Tan, E. M. Greitzer, N. A. Cumpsty, J. J. Adamczyk, and F. E. Marble, "Endwall Blockage in Axial Compressors," *Journal of Turbomachinery*, vol. 121, pp. 499–509, 1999.

[8] B. Lakshminarayana and J. t. Horlock, *Leakage and secondary flows in compressor cascades*. HM Stationery Office, 1965.

[9] I. K. Nikolos, D. I. Douvikas, and K. D. Papailiou, "Theoretical Modelling of Relative Wall Motion Effects in Tip Leakage Flow," in *Volume 1: Turbomachinery*, (Houston, Texas, USA), p. V001T01A017, American Society of Mechanical Engineers, June 1995.

[10] D. A. Rains, *Tip clearance Flows in Axial Compressors and Pumps*. PhD Thesis, California Institute of Technology, Pasadena, California, 1954.

[11] G. T. Chen, E. M. Greitzer, C. S. Tan, and F. E. Marble, "Similarity analysis of compressor tip clearance flow structure," in *ASME 1990 International Gas Turbine and Aeroengine Congress and Exposition*, pp. V001T01A049–V001T01A049, American Society of Mechanical Engineers, 1990.

[12] H. Brandt, L. Fottner, H. Saathoff, and U. Stark, "Effects of the Inlet Flow Conditions on the Tip Clearance Flow of an Isolated Compressor Rotor," in *Volume 5: Turbo Expo 2002, Parts A and B*, (Amsterdam, The Netherlands), pp. 1123–1132, ASMEDC, Jan. 2002.

[13] W. Riéra, J. Marty, L. Castillon, and S. Deck, "Zonal detached-eddy simulation applied to the tip-clearance flow in an axial compressor," *AIAA Journal*, pp. 2377–2391, 2016.

[14] N. Gourdain, F. Wlassow, and X. Ottavy, "Effect of Tip Clearance Dimensions and Control of Unsteady Flows in a Multi-Stage High-Pressure Compressor," *Journal of Turbomachinery*, vol. 134, Sept. 2012. Publisher: American Society of Mechanical Engineers Digital Collection.

[15] C. Montsarrat, *Tip-leakage flow modelling in axial compressors*. PhD Thesis, Université de Lyon, Sept. 2021.

[16] K. Yamada, M. Furukawa, Y. Tamura, S. Saito, A. Matsuoka, and K. Nakayama, "Large-Scale DES Analysis of Stall Inception Process in a Multi-Stage Axial Flow Compressor," in *Volume 2D: Turbomachinery*, (Seoul, South Korea), p. V02DT44A021, American Society of Mechanical Engineers, June 2016.

[17] C. Tan, I. Day, S. Morris, and A. Wadia, "Spike-Type Compressor Stall Inception, Detection, and Control," *Annual Review of Fluid Mechanics*, vol. 42, pp. 275–300, Jan. 2010.

[18] B. Deveaux, C. Fournis, V. Brion, J. Marty, and A. Dazin, "Experimental analysis and modeling of the losses in the tip leakage flow of an isolated, non-rotating blade setup," *Experiments in Fluids*, vol. 61, no. 5, pp. 1–23, 2020. Publisher: Springer.

[19] N. A. Cumpsty, *Compressor aerodynamics*. Longman Scientific & Technical, 1989.

[20] A. Doukelis, K. Mathioudakis, and K. Papailiou, "The effect of tip clearance gap size and wall rotation on the performance of a high-speed annular compressors cascade," *The American Society of Mechanical Engineers*, no. 98-GT-98, pp. 1–8, 1998.

[21] S. Kang and C. H. Hirsch, "Experimental study on the three-dimensional flow within a compressor cascade with tip clearance: Part II—the tip leakage vortex," 1993.

[22] M. Inoue, M. Kuroumaru, and M. Fukuhara, "Behavior of Tip Leakage Flow Behind an Axial Compressor Rotor," *Journal of Engineering for Gas Turbines and Power*, vol. 108, pp. 7–14, Jan. 1986.

[23] J. Katz and A. Plotkin, *Low-Speed Aerodynamics*. 2001.

[24] B. Lakshminarayana and J. Horlock, "Tip-clearance flow and losses for an isolated compressor blade," tech. rep., Aeronautical Research Council Reports and Memoranda, London, 1963.

[25] L. Prandtl, "Tragflügeltheorie," tech. rep., Göttingen Universität, Göttingen, 1919.

[26] C. Montsarrat, B. Deveaux, J. Boudet, J. Marty, and E. Lippinois, "Vortex Lattice Method for the Calculation of the Tip-leakage Flow: Evaluation on a Single Blade," in *ASME TurboExpo 2020*, (Virtual Event), Sept. 2020.

[27] J. Van Geffen and G. F. van Heijst, "Viscous evolution of 2D dipolar vortices," *Fluid dynamics research*, vol. 22, no. 4, pp. 191–213, 1998. Publisher: Elsevier.

[28] H. Lamb, *Hydrodynamics*. University Press, 1932.

[29] I. Delbende and M. Rossi, "The dynamics of a viscous vortex dipole," *Physics of Fluids*, vol. 21, no. 7, p. 073605, 2009. Publisher: American Institute of Physics.

[30] H. B. Squire, *The growth of a vortex in turbulent flow*, vol. 16. ARC, 1954.

[31] P. R. Owen, "The decay of a turbulent trailing vortex," *The Aeronautical Quarterly*, vol. 21, no. 1, pp. 69–78, 1970. Publisher: Cambridge University Press.

[32] A. J. Chorin, "Vortex Sheet Approximation of Boundary Layers," tech. rep., Department of Mathematics and Lawrence Berkeley Laboratory, University of California, 1977.

[33] D. T. C. Porthouse and R. I. Lewis, "Simulation of Viscous Diffusion for Extension of the Surface Vorticity Method to Boundary Layer and Sepa-

rated Flows," *Journal of Mechanical Engineering Science*, vol. 23, pp. 157–167, June 1981.
[34] R. I. Lewis, *Vortex Element Methods for Fluid Dynamic Analysis of Engineering Systems*. Cambridge University Press, 1 ed., Mar. 1991.
[35] B. Deveaux, *Analyse et contrôle de l'écoulement de jeu d'une aube fixe isolée*. PhD thesis, HESAM Université, Ecole Nationale Supérieure d'Arts et Métiers, Nov. 2020.
[36] X. Chen, B. Koppe, M. Lange, W. Chu, and R. Mailach, "Comparison of turbulence modeling for a compressor rotor at different tip clearances," *AIAA Journal*, vol. 60, no. 2, pp. 1186–1198, 2022.
[37] V. Brion, *Stabilité des paires de tourbillons contra-rotatifs: application au tourbillon de jeu dans les turbomachines*. PhD Thesis, 2009.
[38] J. Boudet, A. Cahuzac, P. Kausche, and M. C. Jacob, "Zonal large-eddy simulation of a fan tip-clearance flow, with evidence of vortex wandering," *Journal of Turbomachinery*, vol. 137, no. 6, 2015. Publisher: American Society of Mechanical Engineers Digital Collection.

A Relation between the circulation and the compressor loading

The definition of the circulation writes, with $\boldsymbol{V}$ the velocity:

$$\Gamma = \int_C \boldsymbol{V}\cdot \mathrm{d}\boldsymbol{l} = \int_S \boldsymbol{\omega}\cdot \mathrm{d}\boldsymbol{S}, \tag{11}$$

where C is a closed contour and S the enclosed surface.

Let us express the circulation at the radius r, around a blade of a compressor row of pitch $s(r) = 2\pi r/N_{blades}$, and consisting of N_{blades} blades. Figure 13 indicates in red the contour C chosen around the blade. The curved line BC is a translation of the line AD in the $r\theta$ direction. The length of the two segments AB and CD is $s(r)$.

Equation (11) can be decomposed into four terms, each on one portion of the contour:

$$\Gamma = \Gamma_{AB} + \Gamma_{BC} + \Gamma_{CD} + \Gamma_{DA} \tag{12}$$

By periodicity, the two terms Γ_{BC} and Γ_{DA} cancel each other out since $\Gamma_{BC} = -\Gamma_{DA}$. The pitchwise variations of $V_{\theta 1}$ and $V_{\theta 2}$ are neglected along AB and CD, yielding:

$$\Gamma_{AB} = -s(r)V_{\theta 1} \tag{13}$$

$$\Gamma_{CD} = s(r)V_{\theta 2}, \tag{14}$$

and therefore the circulation is directly proportional to the deflection ΔV_θ:

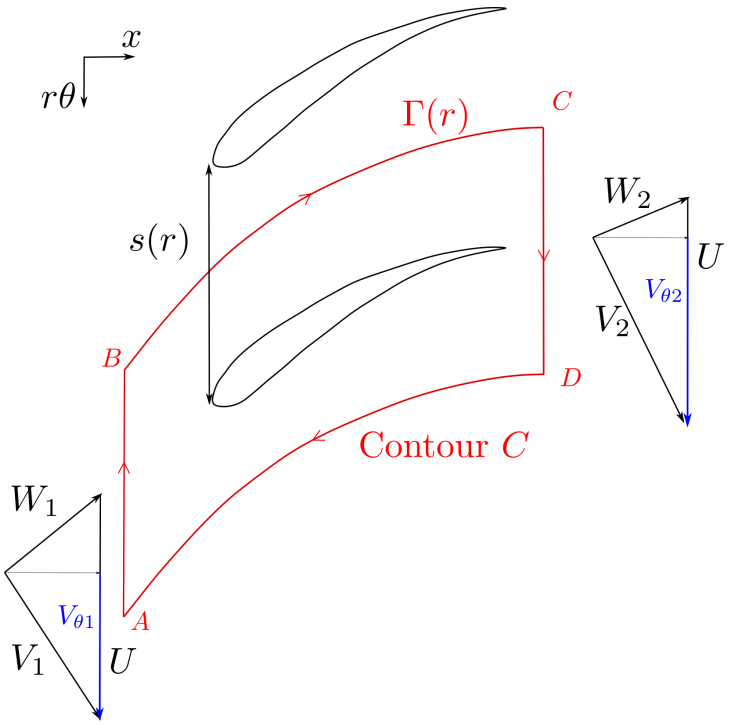

Figure 13: Velocity triangles and integration contour C, at a given radius r, around a compressor blade. $U = r\omega$, with ω the rotation speed of the row.

$$\Gamma(r) = s(r)\Delta V_\theta. \tag{15}$$

According to Euler's equation, for a fixed radius, the blade loading is:

$$\Delta h_0(r) = \Delta(UV_\theta) = r\omega\Delta V_\theta. \tag{16}$$

Therefore, the circulation $\Gamma(r)$ at the radius r is proportional to the blade loading, provided the periodicity assumption over the different passages:

$$\Gamma(r) = s(r)\frac{\Delta h_0(r)}{r\omega} = \frac{2\pi}{N_{blades}\,\omega}\Delta h_0(r) \tag{17}$$